Quaternary Intermetallics Grown from Molten Aluminum: The Homologous Series $Th_2(Au_xSi_{1-x})[AuAl_2]_nSi_2$ (n = 1, 2, 4)

S. E. Latturner,[†] D. Bilc,[‡] S. D. Mahanti,[‡] and M. G. Kanatzidis*[,†]

Departments of Chemistry and Physics, Michigan State University, East Lansing, Michigan 48824

Received September 25, 2001. Revised Manuscript Received January 8, 2002

An appropriate combination of Th or ThO_2 with Au and Si in liquid aluminum has resulted in the formation of three new quaternary intermetallic compounds. All three materials grow as large platelike crystals and have structure types that define a new homologous series. $Th_2AuAl_2Si_3$ is tetragonal, $I4_1/amd$, with unit cell parameters a = 4.2119(4) Å and c = 36.165(5) Å. $Th_2Au_3Al_4Si_2$ and $Th_2Au_5Al_8Si_2$ both crystallize in the orthorhombic space group $Cmmm$, with cell parameters a = 4.266(1) Å, b = 23.574(8) Å, and c = 4.249(1) Å and a = 4.2612(8) Å, b = 35.661(7) Å, and c = 4.2487(8) Å, respectively. The $Th_2(Au_xSi_{1-x})[AuAl_2]_nSi_2$ structures feature planes of parallel infinite zigzag silicon chains alternating with slabs of antifluorite type $AuAl_2$. The $AuAl_2$ slabs increase in thickness going from $Th_2AuAl_2Si_3$ (n = 1) to $Th_2Au_5Al_8Si_2$ (n = 4). All three materials show temperature independent Pauli paramagnetism and metallic conductivity. Band structure calculations were carried out on each compound using density functional theory (full potential LAPW method), and the details of the density of states have been correlated with the observed data.

Introduction

Rare earth or transition metal/main group element compounds have inspired much interest because of the novel crystal structures they often possess and their intriguing electronic and magnetic properties. Increasing the number of elemental components in such materials can lead to more complex structures, and therefore, ternary and quaternary materials may possess properties not found in binary compounds. Furthermore, the additional components add to the tailorability of the electronic properties.[1] These properties can range between semiconducting, in charge-balanced Zintl phases, and metallic, in intermetallic compounds with moderate phase width.[2] For silicides, physical characteristics such as hardness, chemical stability, and high melting point provoke additional interest for uses such as high-temperature furnace components and coatings.[3] Transition metal silicides are also valued as electrical and magnetic materials; some are superconductors,[4] and others have possible applications as thermoelectric components[5] and electrode materials.[6] Aluminides are of similar interest, in particular because of their ubiquitous nature. In commercial aluminum alloys (many of which also contain silicon), rare earths or transition metals are included to improve the properties of the material, forming as yet unexplored multinary intermetallics within the aluminum matrix.[7]

Recent exploration into the use of liquid aluminum and gallium for the synthesis of new ternary and quaternary silicide intermetallics has underscored the power of this method as an alternative to the normal synthesis techniques employed for such materials.[8−12] Silicides are usually synthesized by direct reaction of the elements under vacuum or inert atmosphere. Because of the high melting point of the components, required reaction temperatures are usually over 1500

[†] Department of Chemistry, Michigan State University.
[‡] Department of Physics, Michigan State University.

(1) (a) Buschow, K. H. J. *J. Alloys Compd.* **1993**, *193*, 223. (b) deBoer, F. R.; Zhao, Z. G.; Buschow, K. H. J. *J. Magn. Magn. Mater.* **1996**, *158*, 504−607. (c) Hu, Z.; Yelon, W. B.; Mishra, S.; Long, G. J.; Pringle, O. A.; Middleton, D. P.; Buschow, K. H. J.; Grandjean, F. *J. Appl. Phys.* **1994**, *76*, 443−450.

(2) (a) Nesper, R. *Angew. Chem., Int. Ed. Engl.* **1991**, *30*, 789. (b) Nordell, K. J.; Miller, G. J. *Inorg. Chem.* **1999**, *38*, 579.

(3) (a) Fitzer, E. In *Plansee Proceedings 1955*; Benesovsky, F.; Ed.; Pergamon Press: London, 1956; Chapter 7. (b) Meier, G. H. In *High Temperature Ordered Intermetallic Alloys II*; Stoloff, N. S., Koch, C., Liu, C. T., Izumi, O., Eds.; Materials Research Society Symposium Proceedings 81; Materials Research Society: Pittsburgh, PA, 1987; p 443.

(4) King, R. B. *Inorg. Chem.* **1990**, *29*, 2164−2170 and references therein.

(5) *CRC Handbook of Thermoelectrics*; Rowe, D. M., Ed.; CRC Press: Boca Raton, FL, 1995; and references therein.

(6) (a) Maex, K. *Mater. Sci. Eng. R−Rep.* **1993**, *11*, 53−153. (b) Murarka, S. P. *Silicides for VLSi Applications*; Academic Press: New York, 1983.

(7) (a) Ochiai, S. *Mechanical Properties of Metallic Composites*; Marcel Dekker: New York, 1994. (b) Suresh, S.; Mortensen, A.; Needleman, A. *Fundamentals of Metal Matrix Composites*; Butterworth-Heinemann: Boston, MA, 1993.

(8) Chen, X. Z.; Larson, P.; Sportouch, S.; Brazis, P.; Mahanti, S. D.; Kannewurf, C. R.; Kanatzidis, M. G. *Chem. Mater.* **1999**, *11*, 75−83.

(9) Chen, X. Z.; Sportouch, S.; Sieve, B.; Brazis, P.; Kannewurf, C. R.; Cowen, J. A.; Patschke, R.; Kanatzidis, M. G. *Chem. Mater.* **1998**, *10*, 3202−3211.

(10) Sieve, B.; Chen, X. Z.; Cowen, J. A.; Larson, P.; Mahanti, S. D.; Kanatzidis, M. G. *Chem. Mater.* **1999**, *11*, 2451−2455.

(11) Sieve, B.; Sportouch, S.; Chen, X. Z.; Cowen, J. A.; Brazis, P.; Kannewurf, C. R.; Papaefthymiou, V.; Kanatzidis, M. G. *Chem. Mater.* **2001**, *13*, 273−283.

(12) Sieve, B.; Chen, X. Z.; Henning, R.; Brazis, P.; Kannewurf, C. R.; Cowen, J. A.; Schultz, A. J.; Kanatzidis, M. G. *J. Am. Chem. Soc.* **2001**, *123*, 7040−7047.

10.1021/cm010909w CCC: $22.00
Published on Web 03/13/2002

°C, necessitating use of specialized resistance furnaces, an rf inductive furnace, or an arc welder. Such techniques often result in microcrystalline powders, making structure determination and property measurement difficult. Flux growth facilitates the dissolution of the reactants, optimizing their reactivity and allowing isolation of large crystals. $YNiSi_3$, for instance, was previously only characterized as a polycrystalline powder;[13] the large crystals that are formed in a gallium flux allowed the crystal structure and properties of this compound to be better determined.[8] Exploratory synthesis using a rare earth metal, a first or second row transition metal, and silicon or germanium in liquid aluminum has yielded a number of new phases with rather unusual stoichiometries, such as $Sm_2Ni(Ni_xSi_{1-x})Al_4Si_6$,[9] $RENiAl_4Ge_2$ (RE = Sm, Tb, Y),[10] $RE_4Fe_{2+x}Al_{7-x}Si_8$,[11] and $RE_8Ru_{12}Al_{49}Si_9(Al_xSi_{12-x})$.[12]

We have now extended the scope of our exploration to the third row transition metals. In addition to its noble metal status and unusually high electronegativity,[14] gold is of great interest because of its extensive use in electronics applications. Gold wire−aluminum film connections are often found in semiconductor products, for instance. Studies of the binary intermetallics formed at these junctions have been crucial in optimizing the behavior of these components.[15,16] To facilitate the possible uses of rare earth aluminides and silicides in such applications, it is therefore relevant to investigate the behavior of gold in multinary intermetallic systems. In this work, the combination of gold, silicon, and thorium (or ThO_2) in molten aluminum produced three quaternary intermetallic compounds with new and interrelated structures. Structural relationships between these materials, such as the presence of $AuAl_2$ slabs and one-dimensional (1-D) infinite silicon chains in all three crystal structures, indicate that these compounds can be viewed as members of a new homologous series, $Th_2(Au_xSi_{1-x})[AuAl_2]_nSi_2$, with $n = 1$, 2, and 4.

Experimental Section

Synthesis. In a nitrogen-filled glovebox, Th (Strem, 99.8%), Au (shavings from a 1 oz gold coin, 99.999%), Al pellets (Cerac, 99.99%), and Si powder (Cerac, 99.96%) were combined in a 1:1:10:5 molar ratio (0.232 g of Th, 0.197 g of Au, 0.270 g of Al, and 0.140 g of Si) in an alumina crucible. This was placed into a silica tube 13 mm in diameter, which was sealed under a vacuum of 10^{-4} Torr. This sample was then heated to 1000 °C in 12 h, maintained at this temperature for 15 h, and then cooled to 860 °C in 20 h. It was annealed at 860 °C for 2 days, and slowly cooled to room temperature over 3 days. This allows for the slow crystallization of product out of molten aluminum and any lower-melting eutectics that may be present. The aluminum flux was removed by soaking the crucible in 5 M NaOH for 1 day. The solid product remaining after this isolation procedure included two quaternary compounds; the yield of each based on the initial amount of thorium in the reaction was 40% for $Th_2AuAl_2Si_3$, and 26% for $Th_2Au_3Al_4Si_2$. Single crystals were selected from the product for elemental analysis, X-ray diffraction, conductivity, thermopower, and magnetic susceptibility measurements.

Quaternary intermetallics also form using ThO_2 as a reactant instead of thorium metal. In this case, extra aluminum metal is needed in the synthesis to act as a reducing agent, forming Al_2O_3 presumably in a manner similar to that of the thermite reaction.[17] ThO_2 (Fisher, 99.9%), Au, Al, and Si were weighed into an alumina crucible in a ratio of 1:1:20:5. An inert atmosphere is not necessary for this preparation. The crucible was placed into a silica tube and sealed under vacuum. The heating profile and product isolation was the same as that for the reaction with thorium metal described above. The yields of the three quaternary compounds produced in this reaction, based on the amount of thorium oxide reactant, were approximately 28% for $Th_2AuAl_2Si_3$, 11% for $Th_2Au_3Al_4Si_2$, and 24% for $Th_2Au_5Al_8Si_2$. Additional reactions were carried out at ThO_2/Au/Al/Si ratios of 1:2:30:5 and 1:3:40:5 to observe the effects of changing the reactant mixture; this is discussed in the results section. The thorium and thorium oxide used in this work were depleted and therefore posed no radiation hazard.

EDS Analysis. Selected single crystals were affixed to a SEM plate using carbon tape. Microprobe analysis of these samples was performed using a JEOL JSM-35C scanning electron microscope equipped with a Tracor Northern energy dispersive spectroscopy (EDS) detector. Data were acquired using a 20 kV accelerating voltage and an accumulation time of 50 s. In the analysis of over 100 platelike crystals from both the Th metal and ThO_2 syntheses, three consistent Th:Au:Al:Si elemental ratios were observed: $Th_{2.0}Au_{1.2}Al_{2.0}Si_{2.8}$ (**1**), $Th_{1.9}Au_{2.8}Al_{3.9}Si_{2.3}$ (**2**), and $Th_{1.9}Au_{5.1}Al_{7.7}Si_{2.6}$ (**3**). For all three compounds, the standard deviations of the molar percentages of each element were 5−10%.

X-ray Crystallography. Single-crystal X-ray diffraction data for the three quaternary compounds were collected at room temperature on a Bruker AXS SMART CCD diffractometer. Data processing was then performed using the program SAINT.[18] Because of the highly anisotropic plate shape of the selected crystal of **3**, an analytical absorption correction based on the face-indexed description of the crystal was carried out. The three structures were refined using direct methods with the SHELXTL package of programs.[19] Aluminum and silicon sites were distinguished based on bond lengths (vide infra). Data collection and refinement parameters can be found in Table 1. Atomic positions and occupancy data for all compounds are listed in Tables 2−4. Selected bond lengths and angles for each compound are shown in Table 5. The elemental ratios resulting from the refinements of the three structures were $Th_2Au_{1.26}Al_2Si_{2.74}$ (**1**), $Th_2Au_{2.80}Al_4Si_{2.20}$ (**2**), and $Th_2Au_{4.59}Al_8Si_{2.41}$ (**3**). These will be referred to by the idealized formulae $Th_2AuAl_2Si_3$, $Th_2Au_3Al_4Si_2$, and $Th_2Au_5Al_8Si_2$ respectively.

Magnetic and Electrical Characterization. Magnetic susceptibility measurements were carried out on powders ground from selected single crystals. A Quantum Design SQUID magnetometer was used to collect data from 3 to 300 K. Variable temperature data was collected at a field of 2000 G. The magnetic susceptibility of all three samples showed a linear dependence on field up to the maximum field available (50 000 G). Electrical conductivity measurements were carried out on single crystals using the four-point probe method. Gold paste was used to connect the crystal to four patterned electrodes on a sample holder for an MMR Technologies, Inc. van der Pauw measurement system. Data were collected between 80 and 400 K. Thermopower data were collected on

(13) (a) *CRC Handbook of Crystal Structures and Magnetic Properties of Rare Earth Intermetallics*; CRC Press: Boca Raton, FL, 1994; p 110 and refs 3 and 4 therein. (b) Yarovets, V. I. *Vestn. L'vov. Un-ta. Ser. Khim.* **1977**, 30−34.

(14) Lee, J. D. *Concise Inorganic Chemistry*, 4th ed.; Chapman and Hall: London, 1991; Chapter 27 and references therein.

(15) (a) Kato, H. *Jpn. J. Appl. Phys.* **1986**, *25*, 934−935. (b) Mori, M.; Fukuda, Y.; Kizaki, Y.; Iida, A.; Saito, M. *Electron. Commun. Jpn. 2* **1999**, *82*, 628−636.

(16) (a) Philofsky, E. *Solid-State Electron.* **1970**, *13*, 1391−1399. (b) Selikson, B.; Longo, T. A. *Proc. IEEE* **1964**, *52*, 1638.

(17) Oxtoby, D. W.; Nachtrieb, N. H. *Principles of Modern Chemistry*, 2nd ed.; Saunders College Publishing: Ft Worth, TX, 1990; p 288.

(18) SAINT, version 4. Siemens Analytical X-ray Instruments Inc.: Madison, WI.

(19) Sheldrick, G. M. SHELXTL, Structure Determination Programs, Version 5.0.; Siemens Analytical X-ray Instruments Inc.: Madison, WI, 1995.

Table 1. Crystallographic Data Collection and Refinement Parameters

	$Th_2Au_{1.26}Al_2Si_{2.74}$ (**1**)	$Th_2Au_{2.80}Al_4Si_{2.20}$ (**2**)	$Th_2Au_{4.59}Al_8Si_{2.41}$ (**3**)
fw	799.27	1219.08	1720.93
a (Å)	4.2119(4)	4.266(1)	4.2612(8)
b (Å)	4.2119(4)	23.574(8)	35.661(7)
c (Å)	36.165(5)	4.249(1)	4.2487(8)
V (Å^3)	641.57	427.28	645.64
Z	4	2	2
space group	$I4_1/amd$	$Cmmm$	$Cmmm$
d_{calcd} (g/cm^3)	8.27	9.47	8.85
$2\theta_{max}$ (deg)	75	75	75
μ (mm^{-1})	34.88	43.31	40.11
index ranges	$-7 \le h \le 7$	$-7 \le h \le 7$	$-7 \le h \le 7$
	$-7 \le k \le 7$	$-39 \le k \le 40$	$-60 \le k \le 60$
	$-58 \le l \le 57$	$-7 \le l \le 7$	$-7 \le l \le 7$
no. of reflcns collcd	4742	3395	5090
no. of unique reflcns	466	645	968
R indices ($I > 2\sigma$(I))	$R_1 = 0.0348$	$R_1 = 0.0390$	$R_1 = 0.0391$
	$wR_2 = 0.0834$	$wR_2 = 0.0981$	$wR_2 = 0.0964$
R indices (all data)	$R_1 = 0.0495$	$R_1 = 0.0449$	$R_1 = 0.0401$
	$wR_2 = 0.0901$	$wR_2 = 0.1015$	$wR_2 = 0.0971$
max peak and hole	+5.77, −4.72	+7.04, −3.54	+5.21, −8.45

Table 2. Atomic Positions and Equivalent Isotropic Displacement Parameters (Å^2) for $Th_2AuAl_2Si_3$ (Compound 1)

atom	Wyckoff position	*x*	*y*	*z*	U_{eq}[a]	occupancy
Th	8*e*	0	1/4	0.20252(1)	0.0041(2)	
Au(1)/Si(1)	8*e*	0	1/4	0.08501(2)	0.0043(3)	0.628(5)/0.372(5)
Al(1)	4*b*	0	1/4	3/8	0.0042(9)	
Al(2)	4*a*	0	3/4	1/8	0.0057(9)	
Si(2)	8*e*	0	1/4	0.0161(1)	0.0070(7)	

[a] In this and subsequent tables, U_{eq} is defined as one-third of the trace of the orthogonalized $\mathbf{U}_{ij}$ tensor.

Table 3. Atomic Positions and Equivalent Isotropic Displacement Parameters (Å^2) for $Th_2Au_3Al_4Si_2$ (Compound 2)

atom	Wyckoff position	*x*	*y*	*z*	U_{eq}	occupancy
Th	4*i*	0	0.17722(2)	0	0.0099(2)	
Au(1)/Si(1)	4*j*	0	0.37689(2)	1/2	0.0099(2)	0.898(5)/0.102(5)
Au(2)	2*a*	0	0	0	0.0102(2)	
Al(1)	4*j*	0	0.0617(2)	1/2	0.0124(8)	
Al(2)	4*i*	0	0.4378(2)	0	0.0127(8)	
Si(2)	4*j*	0	0.2739(2)	1/2	0.0123(8)	

Table 4. Atomic Positions and Equivalent Isotropic Displacement Parameters (Å^2) for $Th_2Au_5Al_8Si_2$ (Compound 3)

atom	Wyckoff position	*x*	*y*	*z*	U_{eq}	occupancy
Th	4*j*	0	0.29906(1)	1/2	0.0062(1)	
Au(1)/Si(1)	4*i*	0	0.16560(1)	0	0.0069(2)	0.795(4)/0.205(4)
Au(2)	4*j*	0	0.41630(1)	1/2	0.0068(1)	
Au(3)	2*a*	0	0	0	0.0066(2)	
Al(1)	4*i*	0	0.3758(1)	0	0.0084(6)	
Al(2)	4*i*	0	0.4581(1)	0	0.0084(6)	
Al(3)	4*j*	0	0.1243(1)	1/2	0.0080(6)	
Al(4)	4*j*	0	0.0417(1)	1/2	0.0086(6)	
Si(2)	4*i*	0	0.23400(8)	0	0.0083(5)	

single crystals from 300 to 400 K with an MMR Technologies, Inc. Seebeck measurement system.

Band Structure Calculations. The electronic structure calculations for these compounds were performed within density functional theory (DFT) using the full potential linearized augmented plane wave (LAPW) method implemented in WIEN 97 code.[20] Both a scalar relativistic correction and spin−orbit interaction were included. For the exchange and correlation parts of the potential the Perdew−Burke−Ernzerhof model[21] was used, which incorporates a generalized gradient approximation (GGA). The atomic radii values (in atomic units, 1 au = 0.529 Å) used in the calculations are as follows: 2.5 au for thorium, 2.45 au for gold, 2.2 au for aluminum, and 2.25 au for silicon. Self-consistent iterations were performed with 27 k points in the reduced Brillouin zone with a cutoff between valence and core states of −6.0 Ry; convergence was assumed when the total energy difference between cycles was within 0.0001 Ry.

Results and Discussion

X-ray crystallographic studies show that all three Th/Au/Al/Si intermetallic compounds obtained from reactions in liquid aluminum have common structural motifs. In addition to discussing the reactivity aspects of the flux medium, we will also present a description and analysis of the structural relationships between the three products that indicates they define a new series of homologues with the general formula $Th_2(Au_xSi_{1-x})$-$[AuAl_2]_nSi_2$. Electrical resistivity and magnetic susceptibility studies confirm the metallic nature of these compounds, and indicate subtle variations in the electronic behavior of each. We will also present the results

(20) Blaha, P.; Schwarz, K.; Luitz, J. *WIEN 97: A Full Potential Linearized Augmented Plane Wave Package for Calculating Crystal Properties*; Vienna University of Technology: Vienna, 1997.

(21) Perdew, J. P.; Burke, S.; Ernzerhof, M. *Phys. Rev. Lett.* **1996**, *77*, 3865.

Table 5. Selected Bond Lengths (Å) and Angles (deg)[a]

	$Th_2AuAl_2Si_3$	$Th_2Au_3Al_4Si_2$	$Th_2Au_5Al_8Si_2$
lengths			
Th−Si(2)	3.118(3) (2×)	3.115(3) (2×)	3.146(2) (2×)
	3.187(2) (4×)	3.223(2) (4×)	3.232(1) (4×)
Th−Au(1)	3.2730(4) (4×)	3.2695(7) (4×)	3.2621(4) (4×)
Th−Al		3.454(4)	3.463(3)
Au(1)−Si(2)	2.492(4)	2.428(4)	2.439(3)
Au(1)−Al	2.5546(4)	2.563(3), 2.578(3)	2.585(2), 2.591(2)
Au(2)−Al		2.575(3), 2.589(3)	2.570(2), 2.595(2)
			2.576(2), 2.605(2)
Au(3)−Al			2.592(2), 2.602(2)
Si(2)−Si(2)	2.407(4)	2.412(4)	2.417(3)
angles	122	124	124
Si(2)−Si(2)−Si(2)			

[a] Au(1) refers to the (Au_xSi_{1-x}) disordered site in all three compounds, and Si(2) to the silicon atoms in the zigzag chain.

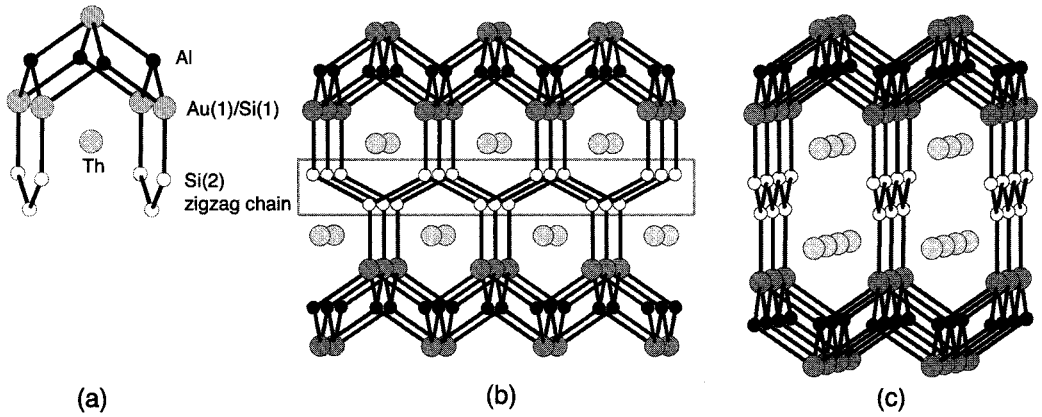

Figure 1. (a) Local coordination environment for thorium in all three structures. (b) The thorium environment linked together to form the fragment that is the basic repeat unit of all the structures investigated in this work. The boxed area is intended to highlight the plane of parallel silicon zigzag chains. (c) View of the same fragment rotated approximately 90°.

of band structure calculations performed at the DFT level in an effort to understand the electronic contributions of each element and to clarify the effects of the common structural motifs on the electronic properties of these materials.

Synthesis. When thorium metal is used in the synthesis, the products consist of a mixture of the two quaternaries $Th_2AuAl_2Si_3$ (comprising about 40% of the solid product after soaking in NaOH) and $Th_2Au_3Al_4Si_2$ (40%), as well as small amounts of Si crystals (10%) and $ThSi_2$ crystals (10%). In the synthesis using ThO_2, the products consist of $Th_2AuAl_2Si_3$ (25%), $Th_2Au_3Al_4Si_2$ (15%), $Th_2Au_5Al_8Si_2$ (45%), Si crystals (5%), and $ThSi_2$ crystals (10%). $Th_2Au_5Al_8Si_2$ was only observed from reactions with ThO_2, possibly due to the lesser availability of the thorium from the initial oxide, or the higher amount of aluminum present in the reaction mixture. Further increasing the amount of aluminum and gold in the synthesis (using ThO_2/Au/Al/Si ratios of 1:2:30:5 or 1:3:40:5 instead of 1:1:20:5) promoted the formation of $Th_2Au_5Al_8Si_2$ to the exclusion of the other quaternary compounds. The products of the oxide synthesis tended to be speckled with small particles of Al_2O_3, which can be removed by sonication. All three quaternary compounds crystallize as large silvery metallic plates up to 2 mm on a side. They are stable in air and moisture and are also resistant to dilute acid (HCl), but they dissolve in aqua regia. EDS is necessary to differentiate the three materials, although spots of gold film on the [010] surface distinguish many of the crystals of $Th_2Au_5Al_8Si_2$.

The reactivity of what normally is a highly stable, refractory oxide (melting point of ThO_2: 3220 °C)[22] under the experimental conditions employed is not only remarkable but also of practical value. The fact that thorium metal can be extracted from the ThO_2 matrix and used productively in this type of synthesis highlights the enormous reducing power of liquid aluminum and implies that many other oxides can be used in a similar fashion. This allows the convenient use of an inexpensive, environmentally stable starting material in molten aluminum chemistry.

Structure Description. Shared Fragments. The structures of the three quaternary compounds show a number of similarities, such as the coordination environment of the thorium atoms, the presence of $AuAl_2$ slabs, and infinite zigzag silicon chains. As shown in Figure 1a, each thorium atom is coordinated to a PbO-like AuAl structure on one side, and silicon chains on the other side. Parts b and c of Figure 1 are different views of how the local coordination sphere of the thorium atoms is linked together horizontally in the quaternary compounds. Vertical stacking of the fragment in Figure 1, parts b and c results in the orthorhombic $CeNiSi_2$ structure shown in Figure 2a, in space group *Cmcm* ($a = 4.141$ Å, $b = 16.418$ Å, $c = 4.068$ Å).[23] The quaternary phases discussed in this work have additional structural features that distinguish them

(22) *CRC Handbook of Chemistry and Physics*; CRC Press: Boca Raton, FL.

(23) Bodak, O. I.; Gladyshevskii, E. I. *Sov. Phys. Crystallogr.* **1970**, *14*, 859.

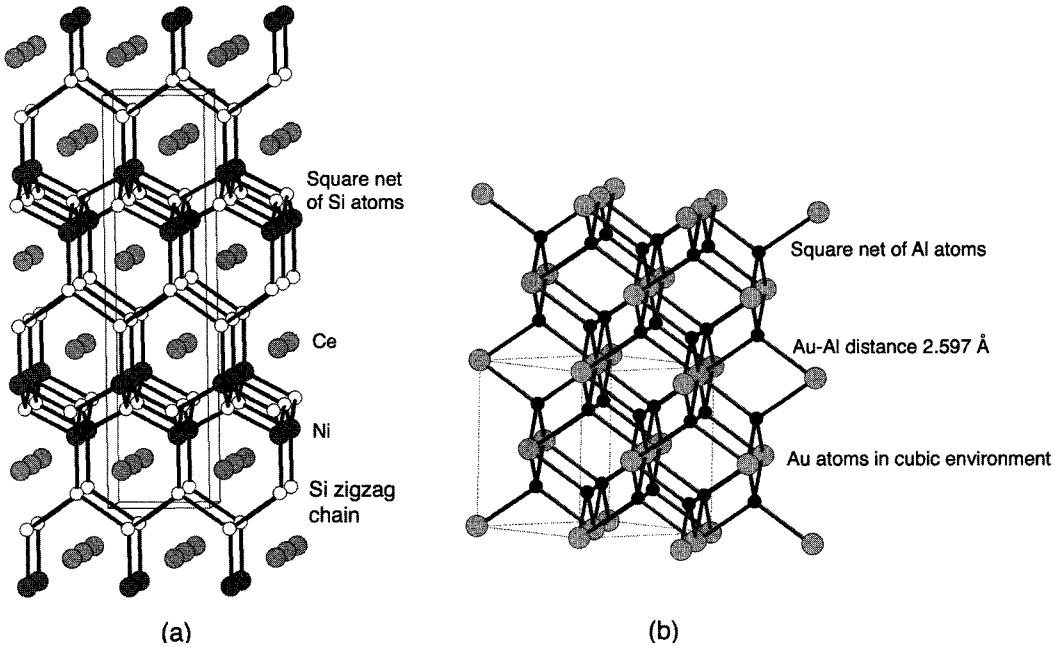

Figure 2. (a) Structure of $CeNiSi_2$ in orthorhombic space group *Cmcm*. (b) Antifluorite structure of $AuAl_2$. The quaternary compounds reported here can be viewed as intergrowths of these two structures.

from this known compound, such as inclusion of $AuAl_2$ slabs. The antifluorite structure of bulk $AuAl_2$ is shown in Figure 2b.[24] The $Th_2(Au_xSi_{1-x})[AuAl_2]_nSi_2$ series members can be described as intergrowths of the $AuAl_2$ and $CeNiSi_2$ structures in a manner analogous to that used by Gladyshevskii et al. to classify a variety of compounds such as $LaNi_{1-x}Ga_6$ and La_2NiGa_{10} as intergrowth structures of $BaAl_4$ and CaF_2.[25]

$Th_2AuAl_2Si_3$. The $Th_2AuAl_2Si_3$ structure, shown in Figure 3, is built from the fragment in Figure 1b; it is stacked vertically, but each section is rotated 90° with respect to the one below it. This results in a new tetragonal structure in space group $I4_1/amd$ ($a = 4.2119$ Å, $c = 36.165$ Å). The silicon zigzag chains are directed along alternating axes: parallel to the *a*-axis in one layer, and parallel to the *b*-axis in the layer above it. This feature bears some resemblance to the structure of $ThSi_2$, which has the same tetragonal space group. $ThSi_2$ has no PbO-type layers and is comprised only of planes of aligned zigzag chains with each plane in alternating directions.

The Au(1)/Si(1) site, found at the "capping" vertexes of the PbO-type layer, is in a square pyramidal environment. It is coordinated to four aluminum atoms defining the pyramid base, and a silicon atom from the zigzag chain at the apex. This site is occupied by a mixture of 63% Au and 37% Si. Complete occupation of this site by gold would result in an elemental ratio of $Th_2Au_2Al_2Si_2$. This was observed in the elemental EDS analysis of a very small number of crystals (the unit cell parameters of which were $a = 4.203(1)$ Å and $c = 36.06(1)$ Å), but the majority of crystals with this structure had the stoichiometry $Th_{2.0}Au_{1.2}Al_{2.0}Si_{2.8}$. The X-ray data also indicated less electron density on this site than would be present for full gold occupancy, so the site was refined as a mixture of Au and Si. The resulting $Th_{2.0}Au_{1.26}Al_{2.0}Si_{2.74}$ stoichiometry is in agreement with the EDS data.

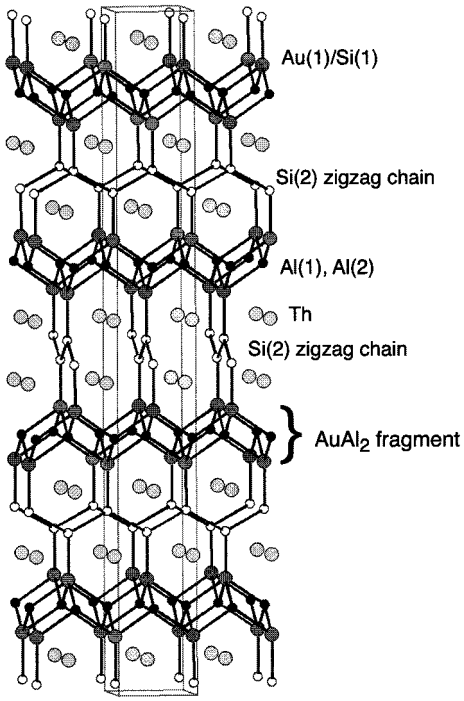

Figure 3. Structure of $Th_2AuAl_2Si_3$ in tetragonal space group $I4_1/amd$. Note that the layers of infinite Si(2) chains are oriented alternately along the *a* and *b* axes.

$Th_2Au_3Al_4Si_2$. The structure of $Th_2Au_3Al_4Si_2$, in orthorhombic space group *Cmmm* ($a = 4.266$ Å, $b = 23.573$ Å, $c = 4.249$ Å), is shown in Figure 4. In this case, the fragments in Figure 1b are linked together vertically through the Au atom vertexes of the PbO-type layer. These gold atoms are surrounded by eight alu-

(24) Villars, P. *Pearson's Handbook, Desk Edition: Crystallographic Data for Intermetallic Phases*; ASM International: Materials Park, OH, 1997; Vol. 1, p 275.

(25) (a) Parthe, E.; Chabot, B. A.; Cenzual, K. *Chimia* **1985**, *39*, 164−174. (b) Grin, Y. N.; Yarmolyuk, Y. P.; Gladyshevskii, E. I. *Sov. Phys. Crystallogr.* **1982**, *27*, 413−419. (c) Yarmolyuk, Y. P.; Grin, Y. N.; Rozhdestvinskaya, I. V.; Usov, O. A.; Kuz'min, A. M.; Bruskov, V. A.; Gladyshevskii, E. I. *Sov. Phys. Crystallogr.* **1982**, *27*, 599−600.

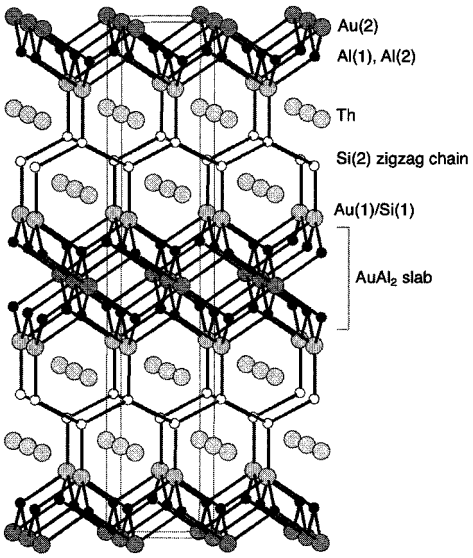

Figure 4. Structure of $Th_2Au_3Al_4Si_2$ in orthorhombic space group *Cmmm*. The Au(2) gold site in the center of the $AuAl_2$ slab is 100% occupied by gold; the capping site of the $AuAl_2$ layer is occupied by a mixture of gold and silicon.

minum atoms in a simple cubic arrangement; the aluminum atoms are tetrahedrally coordinated to four gold (or silicon) atoms. This layer can therefore be described as having an antifluorite-type arrangement, and thus can be regarded as a slab excised out of the lattice of bulk $AuAl_2$, which also has the antifluorite structure as shown in Figure 2b.

This compound can also be viewed as an intercalated modification of the $SmNiSi_3$ structure type. In the $SmNiSi_3$ structure (*Cmmm*, $a = 3.965$ Å, $b = 21.144$ Å, $c = 4.007$ Å),[8] silicon replaces the aluminum in $Th_2Au_3Al_4Si_2$ to form two square net layers. However, unlike in the quaternary compound, these layers are directly linked to each other through Si−Si bonds of 2.348(6) Å, and there is no additional layer of atoms between them to form an antifluorite arrangement. The structural relationship between $SmNiSi_3$ and $Th_2Au_3Al_4Si_2$ is evident in their stoichiometries: $2 \times ThAu(Al_2Si)$ + extra gold site = $Th_2Au_3Al_4Si_2$. As in $SmNiSi_3$, the silicon zigzag chains in $Th_2Au_3Al_4Si_2$ are directed parallel to the *a*-axis.

$Th_2Au_5Al_8Si_2$. $Th_2Au_5Al_8Si_2$ possesses a new orthorhombic structure type shown in Figure 5 (*Cmmm*, $a = 4.2612$ Å, $b = 35.661$ Å, $c = 4.2487$ Å). Again, this quaternary compound is characterized by planes of zigzag silicon chains directed along the *a*-axis. The *b*-axis increases in length from 23.6 to 35.7 Å going from $Th_2Au_3Al_4Si_2$ to $Th_2Au_5Al_8Si_2$. This ~12 Å increase is due to the thicker $AuAl_2$ slabs; it quantitatively represents the incorporation of two $AuAl_2$ unit cells (at 5.99 Å each; see Figure 2b) into the structure. This is also evident in the stoichiometry: addition of two units of $AuAl_2$ to $Th_2Au_3Al_4Si_2$ results in the elemental ratio $Th_2Au_5Al_8Si_2$.

Structural Relationships and the Importance of $AuAl_2$ Blocks. Assignment of elements to the atomic positions in these three structures was straightforward based on expected bond lengths and the results of EDS analysis. The short interatomic distances in the 1-D zigzag chains (close to 2.40 Å for all three materials; see Table 5) strongly indicate that this position is filled

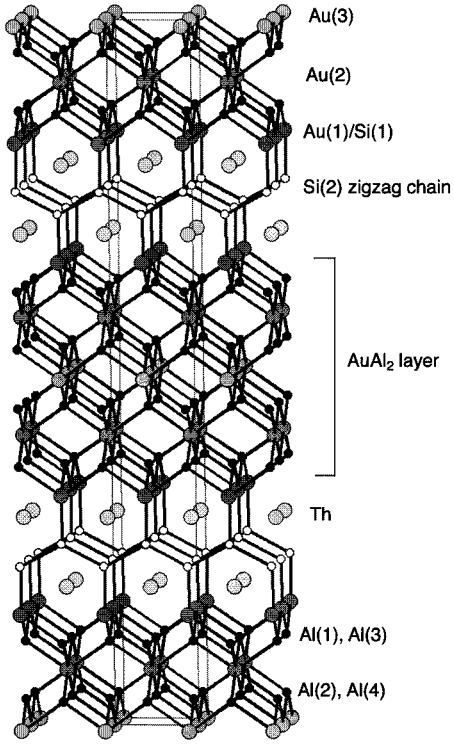

Figure 5. Structure of $Th_2Au_5Al_8Si_2$ in orthorhombic space group *Cmmm*. The two gold sites within the $AuAl_2$ slab (Au(2) and Au(3)) are entirely occupied by gold; the capping site at the edge of this layer is occupied by 80% Au and 20% Si.

by silicon. In other compounds that possess this sort of infinite silicon chain, such as $ThSi_2$, $SmNiSi_2$, and $YNiSi_3$, the Si−Si distances are also around 2.40 Å. Studies on these materials, and on germanium compounds with the same structural feature, have postulated an sp^2 hybridized state for the atoms in the chains and possible π conjugation similar to that in polyacetylene.[8,26] Crystal orbital overlap population (COOP) analyses based on extended Hückel calculations on $LaNiGe_2$ and $YNiSi_3$ indicate that, while the π band is filled, part of the π^* band is also below E_f, lowering the effective bond order in the zigzag chains from a possible 2 to around 1. In these structures, the angle in the chain is close to tetrahedral (109−112°), despite the fact that these tetrelide atoms have trigonal coordination. In the Th/Au/Al/Si quaternaries studied here, this angle is closer to the 120° expected for trigonal sp^2 hybridized silicon (124° in both orthorhombic phases, 122° in the tetragonal phase). This fact may indicate that the silicon chains are more conjugated than those of $YNiSi_3$. However, it is also possible that the larger size of the thorium atoms is responsible for the larger Si−Si−Si angle.

We consider the materials described in this work to be part of a series of phases with stoichiometry $Th_2(Au_xSi_{1-x})[AuAl_2]_nSi_2$. For the tetragonal structure, $n = 1$ and $x = 0.26$, whereas for the two orthorhombic structures with $n = 2$ or 4, x is much higher (between 0.6 and 0.8). The mixed Au_xSi_{1-x} moiety corresponds to the square pyramidal "capping site" of the $AuAl_2$ blocks. Partial occupancy of this site by silicon (instead of

(26) (a) Albert, K.; Meyer, H. J.; Hoffmann, R. *J. Solid State Chem.* **1993**, *106*, 201−210. (b) Proserpio, D. M.; Chacon, G.; Zheng, C. *Chem. Mater.* **1998**, *10*, 1286−1290.

aluminum) is assumed based on EDS results. This is also supported by the fact that these two elements (i.e., Si and Au) are the most highly electronegative in these quaternary compounds. Therefore, while their sizes and chemical behaviors are very different, it is understandable that gold and silicon might share the same crystallographic site in these structures. A similar silicon/late transition metal mixed occupancy site was observed in $Sm_2Ni(Ni_xSi_{1-x})Al_4Si_6$.[9] It is interesting that in the orthorhombic structures of **2** and **3**, the "internal" gold sites of the $AuAl_2$ slabs are fully occupied by gold; it is only in the capping sites on the surface of these slabs where the mixed occupancy occurs. As the $AuAl_2$ slab gets thicker, the bond distances and angles approach those found in bulk $AuAl_2$.[24] The body diagonal of the *ac*-plane approaches the value of 5.997 Å, which is the unit cell edge of the cubic $AuAl_2$ structure. In addition, the Au−Al bonds in the quaternary compounds approach the 2.597 Å length seen in $AuAl_2$ as *n* increases (see Table 5). The orthorhombic symmetry of these compounds is due to the directionality of the silicon zigzag chains. As *n* gets larger, the structure becomes more dominated by the $AuAl_2$ blocks, and thus the *a* and *c* axes of the orthorhombic cell become more similar.

The presence of $AuAl_2$ slabs in the $Th_2(Au_xSi_{1-x})[AuAl_2]_nSi_2$ series is not an isolated incident. Preliminary investigations into a variety of RE/Au/Al/Si systems have resulted in several new intermetallic structures, all of which possess a $AuAl_2$ block.[27] A possible reason for this can be found in early work on Au−Al interfaces on silicon devices. A number of research groups determined that the presence of silicon accelerates the formation of $AuAl_2$ at the expense of other intermetallics such as Au_2Al and Au_4Al. This process incidentally results in an electrical and mechanical degradation at the Au−Al junction, sometimes referred to as the "purple plague" due to the violet color of $AuAl_2$.[16] Similar behavior appears to be at work when gold and silicon are combined with a rare earth or an actinide in liquid aluminum.

Another indication of the possible importance of silicon in the formation of $AuAl_2$ slabs in these intermetallics is the lack of a similar structural motif in RE/Au/Al ternary phases. A survey of the literature on gold-containing ternary aluminides indicates that none of them possess an antifluorite $AuAl_2$ slab.[24,28] $REAuAl_3$ and $REAu_2Al_2$ compounds with the $BaAl_4$ type structure have a trivially small fragment of it, consisting of a square net of aluminum atoms capped on alternating sides by gold atoms (this results in the same kind of PbO-type layer found in $Th_2AuAl_2Si_3$; see Figure 3). However, thicker $AuAl_2$ slabs such as those found in $Th_2Au_3Al_4Si_2$ and $Th_2Au_5Al_8Si_2$ are not found in gold-containing aluminide intermetallics in the absence of silicon. This is a fascinating observation and investigations into the effect of silicon concentration on reaction products of flux growth are currently underway. The $AuAl_2$ fragments that are grown in this environment can potentially be viewed as controllable building blocks (i.e., "synthons") for the design of various intermetallic phases.

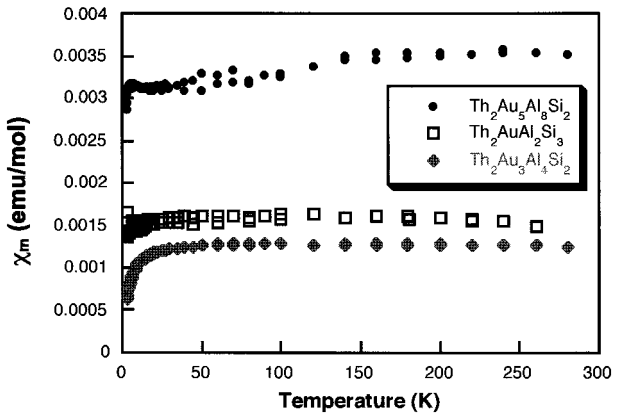

Figure 6. Magnetic susceptibility data for the three $Th_2(Au_xSi_{1-x})[AuAl_2]_nSi_2$ phases, showing temperature independent Pauli paramagnetism.

Magnetic and Electrical Properties. The magnetic susceptibility data for **1**, **2**, and **3** are shown in Figure 6. The molar susceptibilities are low and nearly independent of temperature (features at $T < 40$ K are the result of paramagnetic impurities) for all three materials, indicating that these compounds are intrinsically Pauli paramagnets with no localized spins. The χ_m values of $\sim(1-3) \times 10^{-3}$ emu/mol are in the range observed for other Pauli paramagnetic multinary intermetallics such as $YNiSi_3$ [8] and $Mg_{2-y}(Zn_xAl_{1-x})_{3+y}$.[29] This is an indication that the thorium in the $Th_2(Au_xSi_{1-x})[AuAl_2]_nSi_2$ materials is in a diamagnetic Th^{4+} state, the most stable oxidation state for this metal, or that the thorium orbitals are strongly hybridized with those of other atoms in the structure and the valence electrons are delocalized. The lack of localized spins also indicates that the gold atoms in the structures are diamagnetic. This is not unexpected, since gold is the most electronegative element in these compounds and can therefore fill its d and s orbital shells by accepting electrons from the more electropositive elements. The absence of a magnetic moment on late transition metals is a common feature of many ternary and quaternary aluminum-rich intermetallics;[30] this may be due to the fact that electrons can flow from the rare earth and aluminum atoms to the transition metal, filling its d shell. This idea is supported by the results of band structure calculations, which show the transition metal d orbitals in a narrow set of bands well below the Fermi level.[8−11]

All three compounds show charge transport behavior indicative of metallic systems. The observed Seebeck coefficients are all very small; $Th_2AuAl_2Si_3$ and $Th_2Au_3Al_4Si_2$ have negative coefficients (−5 and −1 μV/K at room temperature, respectively) and $Th_2Au_5Al_8Si_2$ a small positive value (3 μV/K). The electrical conductivity data for the three compounds are shown in Figure 7. The values are in the 5×10^3 S/cm range and an inverse temperature dependence is observed, characteristic of metals. The conductivity is higher and the temperature dependence stronger for $Th_2Au_5Al_8Si_2$, with the other

(27) Latturner, S. E.; Kanatzidis, M. G. Manuscript in preparation.
(28) (a) Miller, G. *Eur. J. Inorg. Chem.* **1998**, 523−536. (b) Nordell, K. J.; Miller, G. J. *Angew. Chem., Int. Ed. Engl.* **1997**, *36*, 2008−2010. (c) Hulliger, F. *J. Alloys Compd.* **1995**, *218*, 255−258. (d) Hulliger, F.; Nissen, H. U.; Wessicken, R. *J. Alloys Compd.* **1994**, *206*, 263−266. (e) Hulliger, F. *J. Alloys Compd.* **1993**, *200*, 75−78.

(29) Lee, C.-S.; Miller, G. J. *J. Am. Chem. Soc.* **2000**, *122*, 4937−4947.
(30) Kirchmayr, H. R.; Poldy, C. A. In *Handbook on the Physics and Chemistry of Rare Earths*; Gschneidner, K. A., Eyring, L. Eds.; North-Holland Physics Publishing: Amsterdam, 1984; Volume 2.

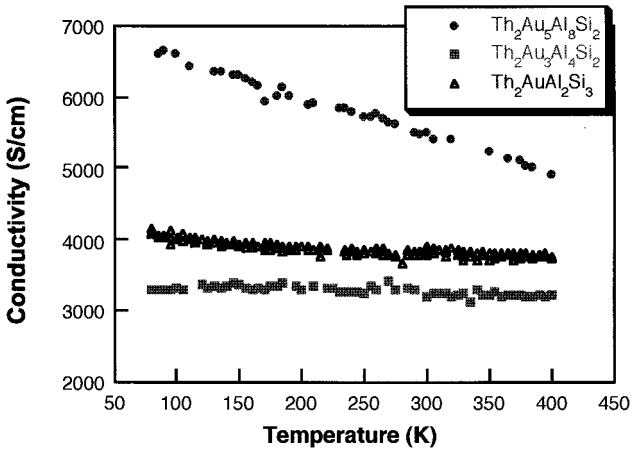

Figure 7. Variable temperature single-crystal electrical conductivity data for the three quaternary compounds. Current flow was parallel to the *ab*-plane.

two compounds showing behavior indicating a higher impurity scattering rate (scattering by defects introduces a largely temperature independent component to the conductivity).[31] While all three structures have mixed occupancy sites, the relative concentration of these Au(1)/Si(1) capping sites is smaller in $Th_2Au_5Al_8Si_2$. The higher conductivity for this compound could also be related to the size of the $AuAl_2$ blocks, since the Au and Al p-orbitals make large contributions to the density of states at the Fermi level for all three $Th_2(Au_xSi_{1-x})[AuAl_2]_nSi_2$ materials (vide infra).

Band Structure Calculations. Band structure studies were carried out on these three compounds in order to shed light on the electronic effects of the $AuAl_2$ slabs, the silicon chains, and the Au_xSi_{1-x} mixed occupancy site. Analysis of the relative contributions of atomic orbitals at the Fermi level also gives insight into the part of the structure that dominates the transport properties of the material. For each compound, partial densities of states were calculated for bands derived from each atom in the structure. The most relevant DOS diagrams are depicted in Figures 8, 10, and 11; the complete data can be found in the Supporting Information.

In the $Th_2(Au_xSi_{1-x})[AuAl_2]_nSi_2$ series, the tetragonal $Th_2AuAl_2Si_3$ compound has the highest amount of occupancy disorder in the Au_xSi_{1-x} site. Because a disordered site cannot be simulated by our calculations, three ordered models of this structure were investigated to explore the effects of substitution on this Au(1)/Si(1) capping site. The first model analyzed was a structure with full gold occupancy, resulting in the stoichiometry $Th_2Au_2Al_2Si_2$. $Th_2AuAl_2Si_3$ can be viewed as a modification of this idealized structure in which silicon is doped into the capping sites. The total and selected partial DOS for $Th_2Au_2Al_2Si_2$ are given in Figure 8. These data reveal the presence of a pseudogap at the Fermi level, indicating that this theoretical compound may be a semimetal. The DOS at E_f is ≈5.1 states/eV per unit cell. Analysis of the partial DOS data shows that the largest contributions at the Fermi level are due to Al-p, Si-p, and Th-d bands. The Au-p bands are located in the range 0 to −3 eV, and are strongly hybridized with

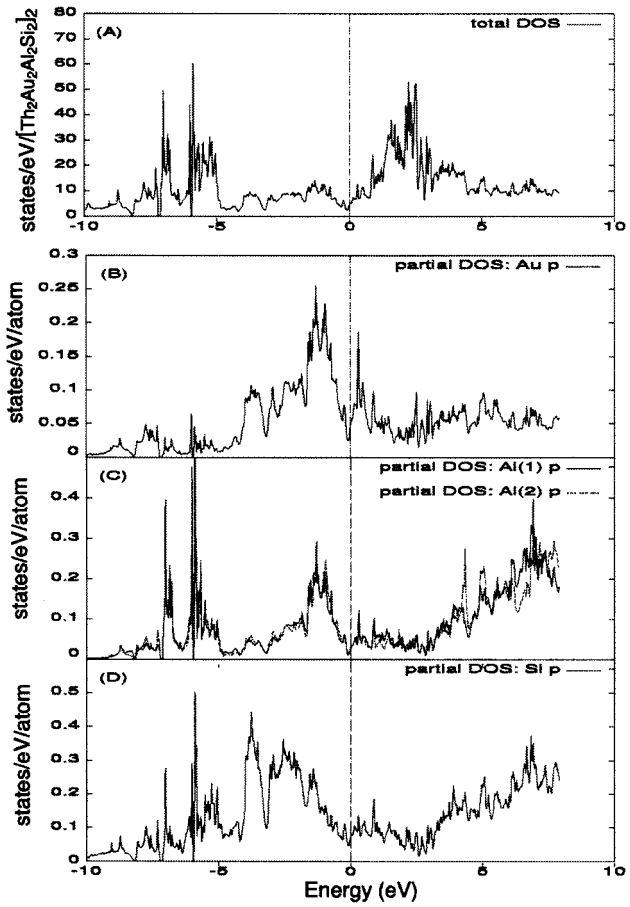

Figure 8. Calculated density of states (DOS) for $Th_2Au_2Al_2Si_2$. The Fermi level E_f is set at 0 eV and is indicated by the dotted line. The total DOS is found at the top in part A, and selected partial DOS data are shown below it in parts B−D.

the Al-p bands. The partial DOS for the two aluminum atoms in the structure are very nearly identical, due to the fact that both atoms have tetrahedral coordination to four Au atoms in $Th_2Au_2Al_2Si_2$.

The Au-d bands are relatively narrow and localized between 5 and 7 eV below E_f, in agreement with the highly electronegative nature of this element. In fact, gold d bands localized at around 6 eV below E_f are a salient feature of all the quaternary compounds studied in this work. This indicates that electron donation from the more electropositive elements results in filling of the gold d-shell, stabilizing these bands. The d bands of gold are also found around 7 eV below the Fermi level in $AuAl_2$.[32] The empty thorium f bands range between 1 and 4 eV above the Fermi level, in agreement with the magnetic susceptibility data indicating fully ionized and diamagnetic thorium (Th^{4+}). Again, this feature is common to all the Th/Au/Al/Si compounds.

To create a model more consistent with the stoichiometry of $Th_2AuAl_2Si_3$, half of the gold atoms in the unit cell of $Th_2Au_2Al_2Si_2$ were replaced by silicon atoms. This changes the symmetry of the compound, giving rise to eight possible space groups, depending on the atoms substituted. Two of the resulting models were selected for investigation: *ortho*-$Th_2AuAl_2Si_3$ (space group *Imma*)

(31) Cox, P. A. *The Electronic Structure and Chemistry of Solids*; Oxford University Press Inc.: New York, 1987; p 99.

(32) (a) Gupta, A.; Gupta, R. S. *Phys. Status Solidi B* **1991**, *168*, 455−465. (b) Hsu, L. S.; Guo, G. Y.; Denlinger, J. D.; Allen, J. W. *J. Phys. Chem. Solids* **2001**, *62*, 1047−1054.

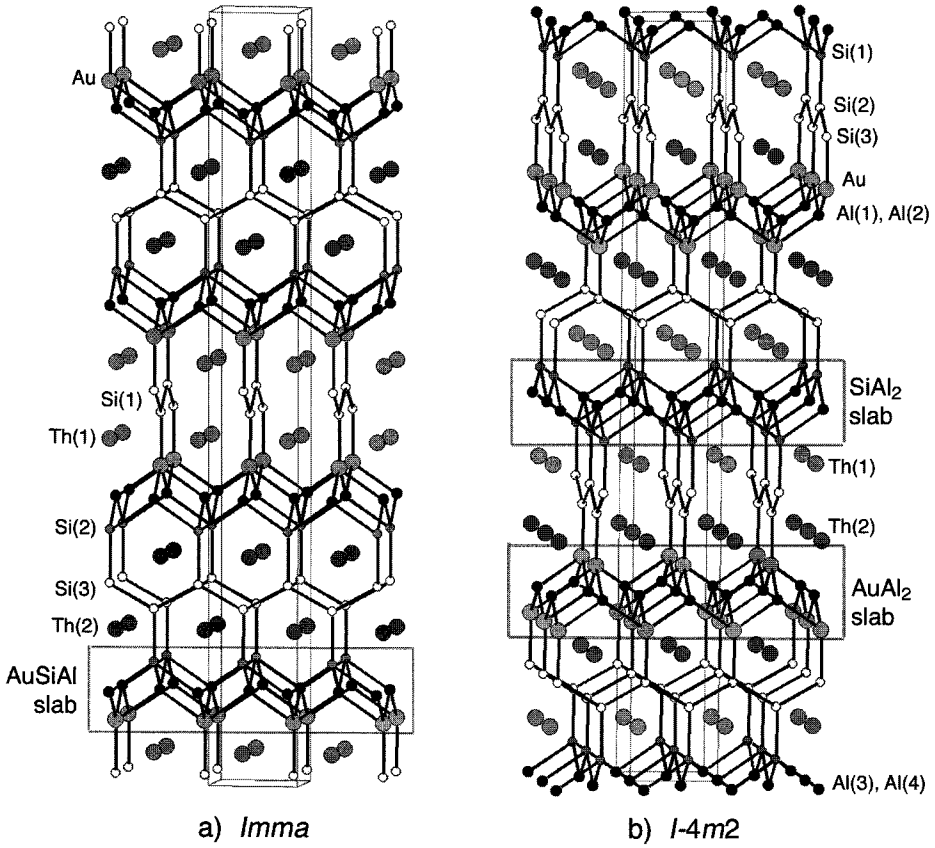

Figure 9. Two models used to approximate the $Th_2AuAl_2Si_3$ stoichiometry: (a) orthorhombic symmetry, space group *Imma*, and (b) tetragonal symmetry, space group *I*-4*m*2. In both models, boxes highlight the $AuAl_2$ fragment slabs with the different silicon and gold occupation of the capping sites.

and *tetra*-$Th_2AuAl_2Si_3$ (space group *I*-4*m*2). These are depicted in Figure 9; a table of the atomic coordinates for these structures is available in the Supporting Information. The DOS diagrams of both models, shown in Figure 10, are very similar and indicative of metallic behavior, in agreement with the observed conductivity data. The DOS at E_f is 6.8 and 10.1 states/eV per unit cell for *tetra*-$Th_2AuAl_2Si_3$ and *ortho*-$Th_2AuAl_2Si_3$, respectively, and there is no pseudogap.

There are subtle differences in the two $Th_2AuAl_2Si_3$ structures and their density of states data that shed light on the source of the pseudogap in the $Th_2Au_2Al_2Si_2$ model. The $AuAl_2$ type fragments in the orthorhombic $Th_2AuAl_2Si_3$ model structure are comprised of a layer of Al atoms bound to Au atoms on one side and Si atoms on the other side, creating in essence a AuAlSi slab. In the tetragonal $Th_2AuAl_2Si_3$ model, on the other hand, there are two types of $AuAl_2$ fragment: an Al layer surrounded by two Au layers (forming a "pure" $AuAl_2$ fragment, with Al(1) and Al(2)), and an Al layer bound by two Si(1) layers (forming $SiAl_2$ slabs, with Al(3) and Al(4)). These structural motifs are highlighted in Figure 9. As mentioned previously, this small portion of the $AuAl_2$ bulk structure is analogous to the PbO-type atomic arrangement. Looking at the DOS for the aluminum atoms (in particular the p-orbital-derived bands), it is notable that in orthorhombic $Th_2AuAl_2Si_3$ these aluminum bands, and those of Au-p and Si(2)-p with which they are hybridized, cross the Fermi level. In the tetragonal $Th_2AuAl_2Si_3$ on the other hand, there are two sets of aluminum p-bands that have distinctly different characteristics. The bands derived from Al(3) and Al(4), both of which are in the $SiAl_2$ slab, have a high DOS at E_f (as does the Si(1)-based band). Al(1) and Al(2), on the other hand, contribute to bands that are concentrated within a region 0−3 eV below E_f along with the Au-p bands. In other words, there is a very low DOS at the Fermi level for all the bands associated with the "pure" $AuAl_2$ slab. This is likely the cause of the pseudogap in the theoretical $Th_2Au_2Al_2Si_2$ material. Addition of silicon into the Au/Si mixed capping site broadens the bands associated with the $AuAl_2$ slab, resulting in a more metallic character.

The silicon bands in $Th_2Au_2Al_2Si_2$ and the two $Th_2AuAl_2Si_3$ derivatives are concentrated in a region 1−5 eV below the Fermi level. In both the $Th_2AuAl_2Si_3$ models, the bands corresponding to the silicon in the capping site (Si(2) in the orthorhombic model, and Si(1) in the tetragonal model) contribute to the lower energy part of the broad p-band DOS compared to the bands derived from the silicon atoms in the zigzag chain. This is understandable given the fact that the capping site interacts with four electropositive aluminum atoms and is therefore stabilized by accepting more electron density. For all three structural models, the Si atoms in the zigzag chain are not strongly hybridized with other atoms, except for slight interactions with thorium d-orbital derived bands just below E_f, and with the gold d-bands in the −5 eV region. This could indicate that the Si 1-D chain is a relatively independent entity in this structure type.

The third model analyzed in the $Th_2(Au_xSi_{1-x})$-$[AuAl_2]_nSi_2$ series was for $x = 0$ and $n = 2$, resulting in the $Th_2Au_3Al_4Si_2$ orthorhombic (*Cmmm*) structure. This

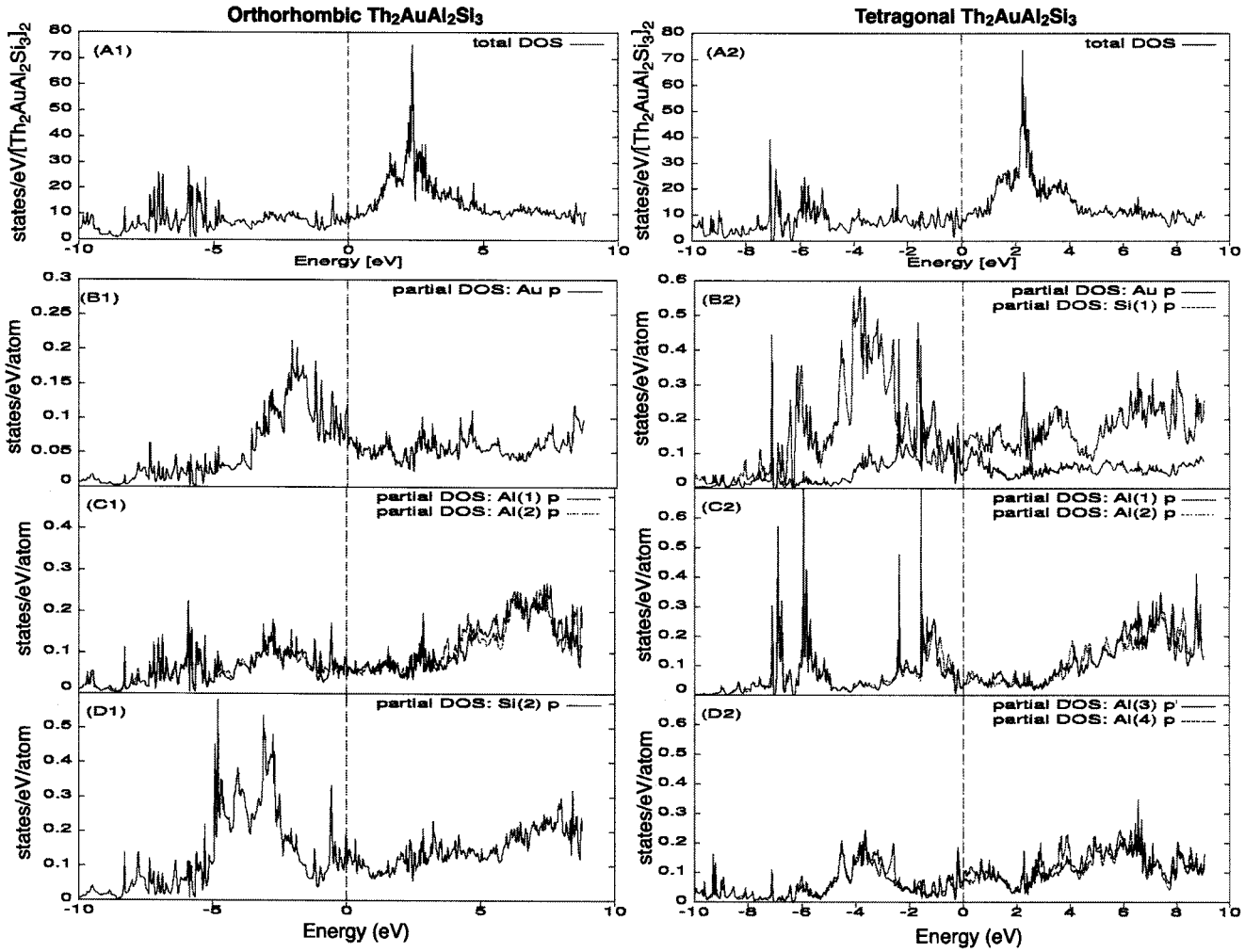

Figure 10. Calculated density of states (DOS) for the two $Th_2AuAl_2Si_3$ models. The diagrams in the left column correspond to the orthorhombic model; those in the right column are for the tetragonal model. The total DOS data for each are at the top, with selected partial DOS shown below. The Fermi level E_f is set at 0 eV and is indicated by the dotted line.

is found to be a metal with a density of states at E_f of 2.7 states/eV; the DOS diagrams are shown in Figure 11. Again, strong interaction is seen between Au-p and Al-p orbitals; these bands are located in the region 0−3 eV below the Fermi level. Also contributing to the DOS at E_f are thorium d-orbital derived bands. The bands derived from the silicon zigzag chains are concentrated in the region between 1 and 4 eV below E_f, with some hybridization with the gold d-orbitals. As in the case of $Th_2Au_2Al_2Si_2$ and its derivatives, the Si-p orbital partial density of states does not show large similarities to the DOS of other atoms in the structure, indicating little interaction with other bands.

The DOS data for $Th_2Au_5Al_8Si_2$, the last member in the $Th_2(Au_xSi_{1-x})[AuAl_2]_nSi_2$ series, are qualitatively similar to those described above. The total DOS at the Fermi level is found to be 5.4 states/eV. As was the case for the other compounds in the series, strong interactions are seen between the aluminum and gold atoms; their overlapping p-orbital derived bands are broader in this case, spanning a range between 4 eV below E_f to 1 eV above E_f. The enlargement of the $AuAl_2$ slab apparently produces a more disperse band that crosses the Fermi level and is likely the cause of the higher electrical conductivity seen for this material. In this case also there is significant Th-d orbital DOS at the Fermi level, and the silicon zigzag chain appears to produce isolated bands in the −1 to −4 eV range.

The magnetic susceptibility and electrical conductivity are both characteristics that are directly proportional to the density of states at E_f. Because $Th_2AuAl_2Si_3$ has twice as many formula units per unit cell ($Z = 4$) as the other two compounds in the series ($Z = 2$), the reported DOS for the two $Z = 2$ structures must be doubled for comparison. This results in the DOS at E_f increasing from $Th_2Au_3Al_4Si_2$ (5.4 states/eV) to $Th_2AuAl_2Si_3$ (in the 6−10 states/eV range), to $Th_2Au_5Al_8Si_2$ (10.8 states/eV). This is consistent with the ordering of the observed values of the magnetic susceptibility (Figure 6) and electrical conductivity (Figure 7), provided that the effect of the disorder in $Th_2AuAl_2Si_3$ is taken into account. Further investigation into this aspect of the band structures is in progress.[33]

These calculations show the strong bonding and energetic stabilization inherent in the $AuAl_2$ structural motif. They suggest that modification of the thickness and composition of this layer can offer significant control over the electronic properties of the materials in which it resides. The partial substitution of silicon for gold in

(33) Bilc, D.; Latturner, S.; Mahanti, S. D.; Kanatzidis, M. G. Manuscript in preparation.

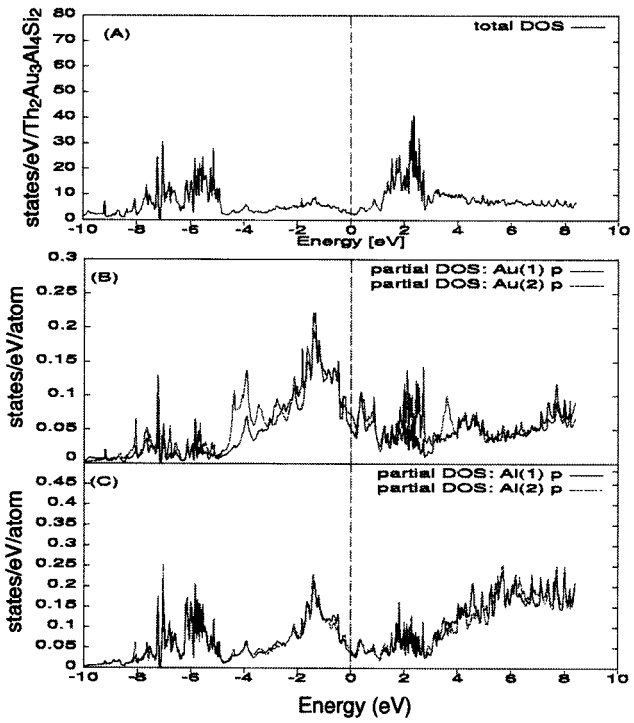

Figure 11. Calculated density of states (DOS) for $Th_2Au_3Al_4Si_2$. The Fermi level E_f is set at 0 eV and is indicated by the dotted line. The total DOS is found at the top, and selected partial DOS data are shown below it.

the capping sites may result in a broadening of the bands at the Fermi level which are associated with the $AuAl_2$ layer. The reason for the apparent necessity of mixed occupancy at this site for all three compounds is still unclear, however. The bands corresponding to the silicon zigzag chains seem to be independent of the electronic manifold of the $AuAl_2$ slabs, instead interacting slightly with bands derived from thorium d-orbitals.

Concluding Remarks

Molten Al has proven to be the key medium for the growth of a homologous series of intermetallics, $Th_2(Au_xSi_{1-x})[AuAl_2]_nSi_2$. The three compounds that were obtained in this series are characterized by planes of parallel silicon chains and antifluorite-type $AuAl_2$ slabs of varying thickness. An unanticipated finding is that the capping sites of the $AuAl_2$ slab exhibit mixed occupancy of gold and silicon. Analysis of DOS data indicates that this (Au_xSi_{1-x}) disorder has a discernible effect on the transport properties of these compounds, as does the thickness of the $AuAl_2$ layer. The presence of this homology possibly forecasts the existence of other higher *n* members in this series. The ubiquitous nature of $AuAl_2$ slabs in these quaternary intermetallics suggests that their formation in aluminum flux may be promoted by the presence of silicon as we are not aware of any ternary RE/Au/Al intermetallics with $AuAl_2$ slabs in their structure. Further investigations into this possible synthetic tool are underway.

Acknowledgment. Financial support from the Department of Energy (Grant DE-FG02-99E45793) is gratefully acknowledged. This work made use of the SEM facilities of the Center for Electron Optics at Michigan State University. We thank B. Sieve, M. Zhuravleva, and P. Larson for useful discussions during the preparation of the manuscript.

Supporting Information Available: Tables giving additional crystal structure data such as anisotropic displacement parameters and complete tables of bond distances and angles for all three compounds and the atomic positions of the two ordered $Th_2AuAl_2Si_3$ model structures studied in the band structure calculations and figures showing complete density of states data for all compounds investigated in this work (PDF). This material is available free of charge via the Internet at http://pubs.acs.org.

CM010909W